Flexible Metal Binding of the Metallo-β-lactamase Domain: Glyoxalase II Incorporates Iron, Manganese, and Zinc in Vivo†

Oliver Schilling,‡ Nathan Wenzel,§ Melissa Naylor,§ Andreas Vogel,‡ Michael Crowder,§ Christopher Makaroff,§ and Wolfram Meyer-Klaucke*,‡

EMBL Outstation Hamburg, Notkestrasse 85, 22603 Hamburg, Germany, and Department of Chemistry and Biochemistry, Miami University, Oxford, Ohio 45056

Received April 28, 2003; Revised Manuscript Received August 12, 2003

ABSTRACT: Glyoxalase II belongs to the metallo-β-lactamase superfamily of proteins, possessing the characteristic dinuclear active site. Within this protein family, glyoxalase II from *Arabidopsis thaliana* is the first member to be isolated with significant amounts of iron, manganese, and zinc when being recombinantly produced in *Escherichia coli*. Enzyme preparations with different ratios of these three metals all yield k_{cat}/K_M values in the range of 1.5−1.9 s^{-1} μM^{-1} with the substrate *S*-D-lactoylglutathione. X-ray absorption spectroscopy reveals binding of all three metals to the dinuclear active site with 5−6-fold coordination consisting of 2.5 ± 0.5 histidine and 2.5 ± 0.5 oxygen ligands. This model does not distinguish site-specific or distributed binding. The metal−metal distance is determined to be 3.18 ± 0.06 Å. Electron paramagnetic resonance spectroscopy gives evidence for several different types of dimetal sites, including spin-coupled Fe(III)Fe(II), Fe(III)Zn(II), and Mn(II)Mn(II) centers. The metal−ligand distances measured by X-ray absorption spectroscopy vary depending on the metal type and comply with their element-specific, characteristic values. This reflects a high degree of structural flexibility within the glyoxalase II dinuclear active site, which is considered as the structural basis for its broad metal selectivity.

The glyoxalase system consists of two enzymes, lactoylglutathione lyase (glyoxalase I, GLX 1)[1] and hydroxyacylglutathione hydrolase (glyoxalase II, GLX 2), that convert 2-oxoaldehydes into 2-hydroxy acids in the presence of glutathione. GLX 1 forms *S*-(2-hydroxyacyl)glutathione from 2-oxoaldehydes in the presence of glutathione, and GLX 2 regenerates glutathione by hydrolyzing *S*-(2-hydroxyacyl)-glutathiones. While the glyoxalase system can utilize a number of 2-oxoaldehydes, the primary physiological substrate of the system is thought to be methylglyoxal, a cytotoxic and mutagenic compound that is formed primarily as a byproduct of carbohydrate and lipid metabolism (*2*, *3*). Methylglyoxal reacts with DNA to form modified guanylate residues (*4*) and interstrand cross-links (*5*) and with proteins to form glycosylamine derivatives of arginine and lysine and hemithioacetals with cysteines (*6*). Therefore, the glyoxalase system plays a critical role in cellular detoxification processes. It has received considerable attention as a possible antitumor and antimalarial target in animal systems (*7*) because rapidly proliferating cell lines and the malaria parasite *Plasmodium falciparum* exhibit high rates of methylglyoxal formation and increased levels of GLX 1 activity. Increased levels of GLX 1 and GLX 2 mRNA and protein have also been detected in tumor cells, including breast carcinoma cells (*8*), while inhibitors of glyoxalases I and II have been shown to inhibit the growth of tumor cells in vitro (*9*, *10*). High levels of methylglyoxal and the glyoxalase enzymes are therefore associated with several aspects of human disease.

A number of early biochemical studies characterized GLX 2 as a nonmetallohydrolase. A more recent study on GLX 2 from *Arabidopsis thaliana* finally demonstrated that the enzyme requires zinc for catalytic activity (*11*). GLX 2 enzymes share conserved amino acids known to bind zinc in the metallo-β-lactamases (*12*, *13*). The crystal structure of human GLX 2 (*14*), with more than 50% sequence identity to the *A. thaliana* enzyme, reveals an overall structure and a dizinc active site characteristic for the metallo-β-lactamase superfamily. Interestingly the authors report the presence of about 0.7 equiv of iron in addition to 1.5 equiv of zinc but model the enzyme with two zinc ions (*14*). More information on the GLX 2 metal binding properties has emerged from mutational studies on the human (*15*−*17*) and plant enzymes (*18*). Of particular interest to the present study is the observation that the cytoplasmic isoform of *A. thaliana* GLX 2 (GLX 2-2)[2] can have a dinuclear zinc−iron center (*18*).

† This work was supported in part by National Science Foundation Grant MCB-9817083.

* To whom correspondence should be addressed. Tel: +49 40 89902124. Fax: +49 40 89902149. E-mail: wolfram@embl-hamburg.de.

‡ EMBL Outstation Hamburg.

§ Miami University.

[1] Abbreviations: GLX 1, glyoxalase I; GLX 2, glyoxalase II; GLX 2-2, cytoplasmic glyoxalase II isozyme; EPR, electron paramagnetic resonance; EXAFS, extended X-ray absorption fine structure; Fe-med GLX 2-2, GLX 2-2 produced in iron-enriched medium; Mn-med GLX 2-2, GLX 2-2 produced in manganese-enriched medium; MOPS, 4-morpholinepropanesulfonic acid; SLG, *S*-D-lactoylglutathione; std-med GLX 2-2, GLX 2-2 produced in medium without metal addition; XAS, X-ray absorption spectroscopy.

[2] The EC number for *Arabidopsis thaliana* GLX 2-2 is 3.1.2.6; the Swiss-Prot primary accession number is 024496.

10.1021/bi034672o CCC: $25.00
Published on Web 09/20/2003

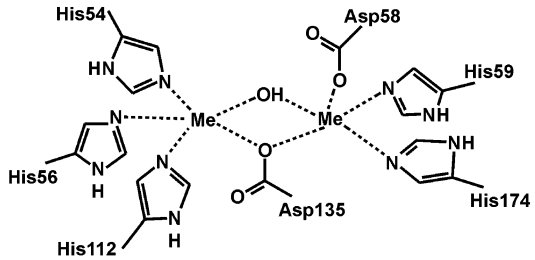

FIGURE 1: Dinuclear active site model for *A. thaliana* GLX 2-2. This model is derived from the crystal structure of human GLX 2 (*14*); all metal ligating residues are conserved in *A. thaliana* GLX 2-2. M = metal (iron, manganese, or zinc); the model implies neither site-specific nor distributed binding.

Mutations inside and outside the metal binding region affect the relative amounts of bound metal (*18*). This observation raises a number of questions concerning the structure of the metal site and its role in *A. thaliana* GLX 2-2 as well as more general questions concerning the specificity of metal binding domains. Typically, members of the metallo-β-lactamase superfamily have one metal binding site with three conserved ligating histidine residues while the metal coordination in the other site is less conserved. The crystal structure of human GLX 2 showed, in addition to the three conserved histidines of one site, a bridging aspartate and a bridging water (*14*). The metal in the less conserved site is coordinated by two histdines, two aspartates, and two water molecules. The metal binding residues of human GLX 2 are conserved in *A. thaliana* GLX 2; the coordination environment is therefore expected to be structurally similar (Figure 1).

Within the metallo-β-lactamase superfamily, enzymes with β-lactamase activity require one or two zinc ions for enzymatic catalysis (*19*), zinc phosphodiesterase from *Escherichia coli* requires two zinc ions for full phosphodiesterase activity (*20*), glyoxalase II enzymes bind zinc, iron, and manganese (*18*; this report), while the rubredoxin:oxygen oxidoreductase contains a diiron center and is unique in possessing only two histidines in the first binding site (*21*). Depending on its context, the metallo-β-lactamase fold is capable of binding several different metals.

The present study focuses on the *in vivo* metal utilization of glyoxalase II. Recombinant *A. thaliana* GLX 2-2 has been isolated with different ratios of *in vivo* bound iron, manganese, and zinc. Steady-state kinetic analysis determines the catalytic competence, X-ray absorption spectroscopy reveals active site metal binding properties, and electron paramagnetic resonance illuminates the dinuclear metal−metal combinations. The biochemical and spectroscopic results give rise to the first structural and functional characterization of a member of a metallo-β-lactamase domain with active site bound iron, manganese, and zinc.

MATERIALS AND METHODS

General. S-D-Lactoylglutathione (SLG) was purchased from Sigma-Aldrich (St. Louis, MO). All chromatographic steps were performed on an Amersham Biosciences (Piscataway, NJ) fast protein liquid chromatography system operating at 4 °C. Metal standards were purchased from Fisher Scientific (Pittsburgh, PA) and were diluted with Nanopure-purified water (Barnstead, Dubuque, IA). All other chemicals used in this study were purchased commercially and were of the highest quality available.

Overexpression and Purification. The cytoplasmic glyoxalase II isozyme GLX 2-2 from *A. thaliana*, recombinantly produced in *E. coli*, was used for this study. Overexpression and purification were performed as described previously (*18*), using the pT7-7/GLX 2-2 expression plasmid (*11*) in BL21-(DE3)pLysS *E. coli* cells, grown in ZY medium [2.0% (w/v) tryptone, 1.5% yeast extract, 0.5% sodium chloride, 1.0% (v/v) glycerol (*18*)]. To produce metal-enriched enzyme species, 0.25 mM manganese chloride or 0.25 mM ferrous ammonium sulfate was added to the medium, yielding iron medium and manganese medium GLX 2-2 (Fe-med GLX 2-2 and Mn-med GLX 2-2, respectively). GLX 2-2 from bacterial growth medium without additional metal is referred to as standard medium GLX 2-2 (std-med GLX 2-2).

Protein Concentration. Enzyme concentrations were determined by measuring the A_{280nm} and using the extinction coefficient $\epsilon_{280nm} = 37584\ M^{-1}\ cm^{-1}$, established using the method of Edelhoch (*22*). Previous studies about GLX 2 enzymes used a variety of different extinction coefficients. The value used in this report has been confirmed by additional methods, such as comparative analysis of the metal content with proton-induced X-ray emission (unpublished results).

Steady-State Kinetics. Steady-state kinetic parameters were determined by measuring the hydrolysis rate of SLG at 240 nm in 10 mM 4-morpholinepropanesulfonic acid (MOPS) buffer, pH 7.2, at 25 °C with a Hewlett-Packard (Agilent Technologies, Loveland, CO) 8453 diode array UV−vis spectrophotometer; essentially as previously described (*11*). Measurements were performed at least in triplicate. Kinetic constants were determined using Curvefit version 0.7e (GraphPad Software, San Diego, CA).

Metal Analysis. The metal content of the GLX 2-2 samples was measured with a Varian (Palo Alto, CA) inductively coupled plasma spectrometer with atomic emission spectroscopy detection. Purified enzymes were diluted with 10 mM MOPS, pH 7.2, to a concentration of 10 μM and analyzed for zinc, manganese, iron, copper, nickel, and cobalt. The metal content data presented in this paper represent an average from at least three preparations of each growth condition.

X-ray Absorption Spectroscopy. X-ray absorption spectra at the iron, manganese, and zinc K-edge were gathered for GLX 2-2 overexpressed in standard or metal-enriched medium. Lyophilized protein was filled into plastic sample holders covered with Kapton windows, frozen in liquid nitrogen, and kept at 30 K during the experiment. Spectra were collected in fluorescence mode at the EMBL bending magnet beamline D2 (DESY, Hamburg, Germany), equipped with a Si(111) double crystal monochromator, a focusing mirror, and a 13-element Ge solid-state detector. The Bragg reflections of a static Si(220) crystal in back-reflection geometry served for the absolute energy calibration of the iron and zinc spectra (*23*); potassium permanganate ($KMnO_4$) served as a reference system for the relative energy calibration of the manganese spectra. Data reduction was performed with the EXPROG software package (C. Hermes and H. F. Nolting, EMBL, Hamburg, Germany) with $E_{0,Mn} = 6540$ eV,

Table 1: Glyoxalase II Metal Contents Reported in Previous Studies

enzyme	metal (mol/mol of protein) iron	manganese	zinc	ref
human GLX 2, wild type	0.7	not tested	1.5	*14*
A. thaliana GLX 2-2, wild type	0.8	not tested	0.4	*18*[a]
A. thaliana GLX 2-2, R248W mutant	0.4	0.1	2.1	*11*[b]

[a] The protein concentration in ref *18* was originally determined with a protein extinction coefficient different from the one used in our current study. Adjustment of the previously reported metal content yields the values stated in this table. [b] Additionally, a content of 0.5 nickel equivalents per protein was reported.

$E_{0,Fe} = 7120$ eV, and $E_{0,Zn} = 9660$ eV. The extended X-ray absorption fine structure (EXAFS) spectra were analyzed with EXCURV98, applying constrained refinement (*1*). Ligand types and coordination numbers were varied manually; distances, Debye−Waller factors, and the Fermi energy offset were refined by the software. The area of the preedge peak at the normalized iron absorption edge was determined as described by ref *24*.

Electron Paramagnetic Resonance Spectroscopy. Electron paramagnetic resonance (EPR) spectra were recorded on a Bruker Instruments (Billerica, MA) ER 300 spectrometer equipped with an ER 035M NMR gaussmeter and a Hewlett-Packard 5352B microwave frequency counter. Double integration of EPR spectra was performed with the ESP 300 software package from Bruker Instruments. $CuSO_4$, $[Fe(NH_4)_2]SO_4$, $MnCl_2$, and $FeCl_3$ were used as spin-quantitation standards for Cu(II), Fe(II), Mn(II), and Fe(III), respectively. Perpendicular mode EPR spectra were measured at 4.7 K with the following settings: 2 mW microwave power, 9.48 GHz microwave frequency, 10 G modulation amplitude, 100 kHz modulation frequency, sweep time of 41.9 s, receiver gain of 10^5, 41 ms conversion time, 82 ms time constant, 41.9 s sweep time, center field at 3350 G, and the sweep width at 6400 G. Air-oxidized GLX 2-2 samples from standard or metal-enriched medium were placed into 4 mm quartz EPR tubes and frozen by slow immersion of the EPR tubes into liquid nitrogen.

RESULTS

Metal Content and Catalytic Activity of Recombinant GLX 2-2

Previous studies on GLX 2 have reported a number of different values for the metal equivalents per protein for the recombinant enzymes (Table 1). In general, the wild-type forms of both human and plant glyoxalase II were isolated with significant but varying amounts of iron and zinc. To probe the potential flexibility of the metal center in GLX 2-2, we have studied the metal content of *A. thaliana* GLX 2-2 when it is overexpressed in the presence of added metal ions. It has so far not been possible to produce glyoxalase II with only one type of metal from previously metal-depleted samples, because the enzyme precipitates in the presence of chelating agents such as ethylendiaminetetraacetic acid (EDTA) (*11*).

In this study, enzyme produced in rich medium (std-med GLX 2-2) yields a metal content of 0.8 ± 0.2 iron, 0.4 ± 0.2 zinc, and 0.30 ± 0.05 manganese per protein (Table 2). This confirms previous findings for plant glyoxalase II (Table 1). Substoichiometric metal occupancy is to be expected for "as isolated" recombinant proteins and may be attributed to loss of metal during purification or to limited metal availability during overexpression. Std-med GLX 2-2 exhibits a k_{cat} of 408 ± 103 s^{-1}, a K_M of 220 ± 60 μM, and thus a k_{cat}/K_M value of 1.9 s^{-1} μM^{-1} with the substrate SLG. Overexpression of GLX 2-2 in rich medium with 0.25 mM manganese chloride yields enzyme with 1.3 ± 0.5 manganese, 0.4 ± 0.1 iron, and 0.06 ± 0.03 zinc per protein (Mn-med GLX 2-2). The kinetic constants k_{cat} (168 ± 39 s^{-1}) and K_M (115 ± 25 μM) of Mn-med GLX 2-2 are approximately half of the values observed for std-med GLX 2-2. The catalytic efficiency (k_{cat}/K_M) has a value of 1.5 s^{-1} μM^{-1}, similar to std-med GLX 2-2, despite the altered metal composition and changes of the individual k_{cat} and K_M values for Mn-med GLX 2-2. The decrease of both k_{cat} and K_M correlates to some extent with the decrease of protein-bound iron. However, the present samples, containing a mixture of iron, manganese, and zinc, are too complex to finally establish the catalytic functionality of individual metal types. Overexpression of GLX 2 in rich medium containing 0.25 mM ferrous ammonium sulfate leads to metal composition and kinetic properties comparable to those of std-med GLX 2-2. This may partially be due to oxidation of the added ferrous iron to barely soluble ferric iron in the growth medium, a process that is favored by the intense aeration of the bacterial culture. The k_{cat}/K_M values of std-med, Fe-med, and Mn-med GLX 2-2 ($1.5-1.9$ s^{-1} μM^{-1}) are of the same order of magnitude as those previously reported in the literature [4.2 s^{-1} μM^{-1} for human and 4.7 s^{-1} μM^{-1} for *A. thaliana* GLX 2 (*25*, *26*)].

X-ray Absorption Spectroscopy Reveals Binding of Iron, Manganese, and Zinc to the Dinuclear Active Site

In this study, X-ray absorption spectroscopy (XAS) is used to prove the location of iron, manganese, and zinc in the GLX 2-2 dinuclear active site (Figure 1). XAS allows the element-specific characterization of metal sites in biological

Table 2: Steady-State Kinetic Constants and Metal Contents of GLX 2-2 Samples[a]

sample	substrate: SLG k_{cat} (s^{-1})	K_M (μM)	k_{cat}/K_M (s^{-1} μM^{-1})	metal (mol/mol of protein) iron	manganese	zinc
std-med GLX 2-2	408 ± 103	220 ± 60	1.9	0.8 ± 0.2	0.30 ± 0.05	0.4 ± 0.2
Fe-med GLX 2-2	359 ± 109	220 ± 110	1.6	0.8 ± 0.2	0.30 ± 0.05	0.3 ± 0.1
Mn-med GLX 2-2	168 ± 39	115 ± 25	1.5	0.4 ± 0.1	1.3 ± 0.5	0.06 ± 0.03

[a] Both the metal content and the steady-state kinetics are determined as described in the Materials and Methods section. Values are the average ± standard deviation; measurements are from at least three protein preparations. Copper, nickel, and cobalt were not detected for any of the preparations.

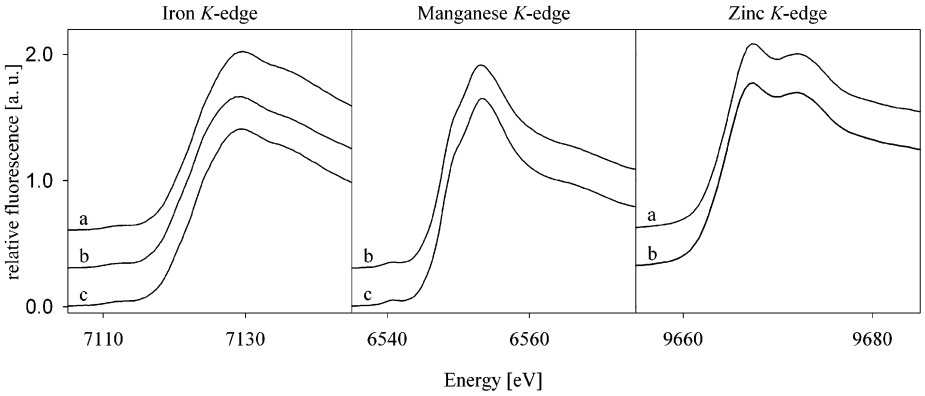

FIGURE 2: Normalized iron, manganese, and zinc absorption edges: a, GLX 2-2 produced in standard medium; b, GLX 2-2 produced in iron-enriched medium; c, GLX 2-2 produced in manganese-enriched medium; au, arbitrary units. The normalized K_α fluorescence is shown. Spectra for components a and b have an offset of +0.6 and +0.3, respectively.

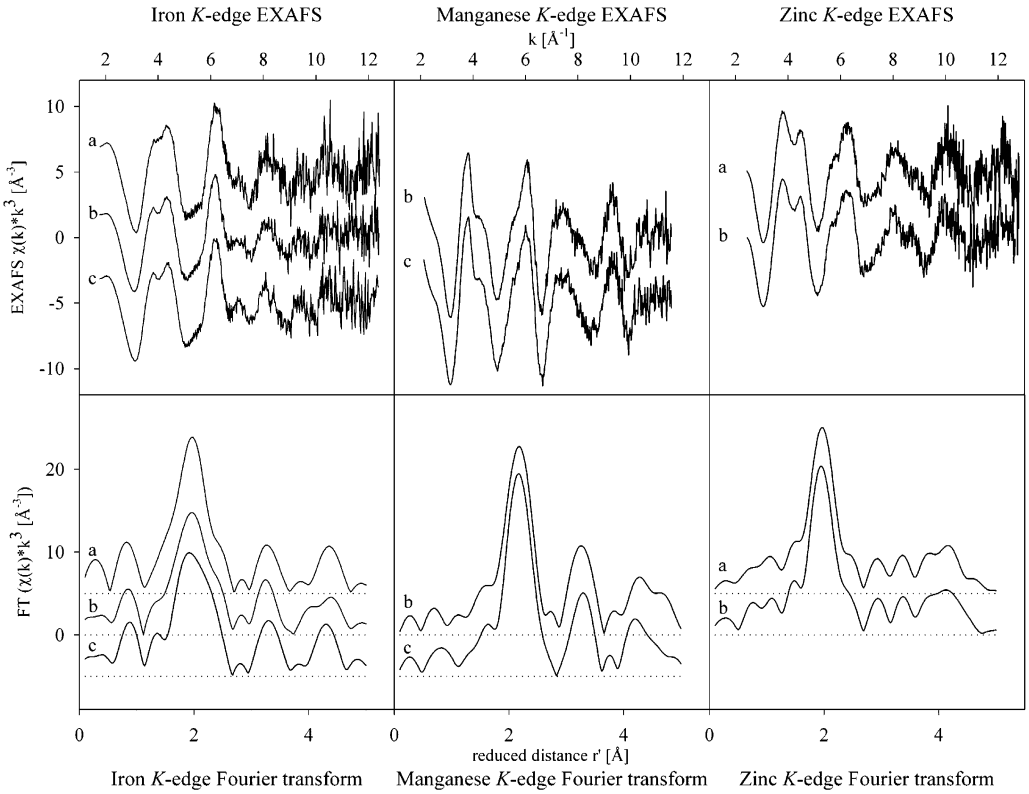

FIGURE 3: EXAFS spectra and Fourier transform from GLX 2-2 preparations with different ratios of iron, manganese, and zinc: a, GLX 2-2 produced in standard medium, offset +5; b, GLX 2-2 produced in iron-enriched medium, no offset; c, GLX 2-2 produced in manganese-enriched medium, offset −5. The metal contents of the individual EXAFS samples are (a) 0.5 iron, 0.3 manganese, and 0.4 zinc per protein; (b) 0.8 iron, 0.3 manganese, and 0.2 zinc per protein; (c) 0.6 iron, 0.7 manganese, and 0.0 zinc per protein (error range: ±10%). Manganese EXAFS for std-med GLX 2-2 is not presented due to a very high noise level; zinc EXAFS for Mn-med GLX 2-2 has not been recorded due to the low zinc content. $\chi(k)$ = EXAFS amplitude. Fourier transform was performed with the EXCURV98 software, applying the Fermi energy offset values stated in Table 3 and phase shift corrected for the first shell, yielding the reduced distance r'. Dotted lines indicate the zero for each Fourier transform.

systems, yielding information about the types and distances of coordinating ligands as well as the oxidation state of the metal center. For multinuclear proteins, the metal−metal distance can also be determined.

The different EXAFS spectra for each individual metal are generally in phase and possess similar features, such as a double peak at about 4 $Å^{-1}$ (Figure 3). The iron EXAFS of std-med GLX 2-2 has some minor differences at ca. 4, 7, and 11 $Å^{-1}$. These differences are not structurally significant. Moreover, std-med and Fe-med GLX 2-2 have very similar EPR spectra (Figure 5) in accordance with their identical iron content. The variations observed for the std-med iron EXAFS may be due to a higher noise level. The element-specific Fourier transformed EXAFS spectra show a high degree of similarity as well. There are some deviations for the iron EXAFS Fourier transform, due to elevated noise levels at high *k*-values.

The double peak feature at about 4 $Å^{-1}$ is indicative of multiple scattering effects. In proteins, this effect is mostly caused by metal ligation to histidine residues (*1*). The zinc EXAFS has significant similarity to spectra recorded for other metallo-β-lactamase-like proteins, such as the binuclear zinc phosphodiesterase from *E. coli* (*20*). For all three metals, the EXAFS Fourier transform shows a neighboring metal

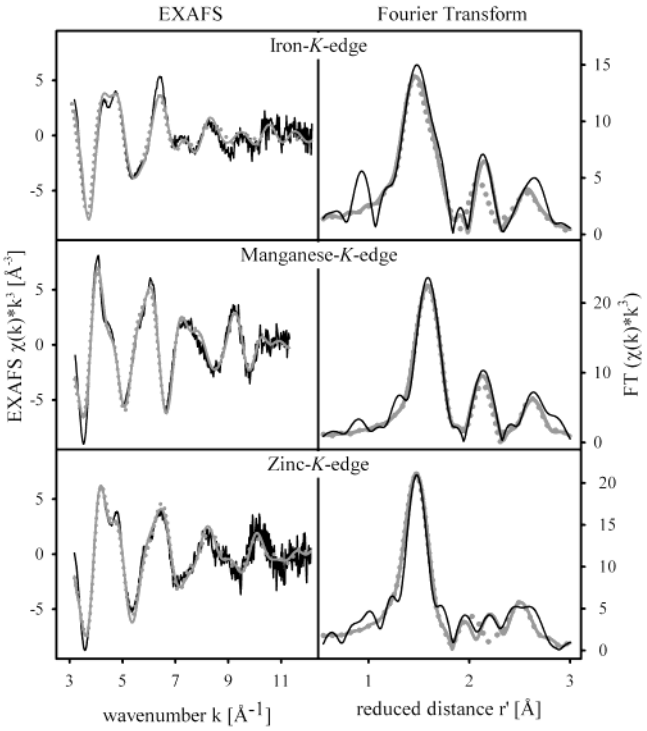

FIGURE 4: Model fits of the EXAFS spectra. Experimental data are represented by thin black lines while thick black lines represent spectra calculated for the metal-specific models given in Table 3. Dotted gray lines represent spectra calculated for refined models without a neighboring metal; these models are tabulated as Supporting Information. The experimental spectra shown in Figure 3 are averaged to reach a better signal-to-noise ratio. Std-med iron EXAFS has not been included as discussed in the text. $\chi(k)$ is the EXAFS amplitude; r' is the metal−ligand distance corrected for first-shell phase shifts; au = arbitrary units; FT = Fourier transform amplitude.

ion at about 3.2 Å (Figure 3). For zinc, in contrast to iron and manganese, this feature is less obvious but still indicative of a neighboring metal as is discussed below. Taken together, XAS proves the binding of iron, manganese, and zinc to the glyoxalase II dinuclear active site. Despite their similar coordination environment, iron, manganese, and zinc have different individual EXAFS spectra. This is attributed to metal-specific variations of the first-shell distance. Iron, manganese, and zinc have different characteristic coordination bond lengths, ranging from 2.0 Å (zinc−oxygen) to 2.2 Å (manganese−oxygen) (*27*). Accordingly, the first-shell peaks of the EXAFS Fourier transform have different, element-specific positions (Figure 4).

Metal-Specific Bond Lengths Reveal Structural Flexibility of the Active Site. The element-specific spectra were grouped together for EXAFS analysis with the exception of std-med GLX 2-2 iron EXAFS. The latter spectrum has not been included due to the small deviations discussed above. The two metal binding sites of glyoxalase II differ essentially by one histidine residue (Figure 1). Quantitative EXAFS analysis determines coordination numbers with an accuracy of 20% as has been found by a reference study on model compounds (*28*). Hence, the present data do not distinguish distributed binding from site-specific binding: distributed binding has an average ligation of 2.5 histidines; the 20% error range of the coordination number includes site-specific location in the 2 His or 3 His site. To avoid overinterpretation of the data, the spectra are fitted with a model of 2.5 ± 0.5 histidine residues and 2.5 ± 0.5 oxygen ligands. The noninteger coordination numbers reflect the intrinsic error range of EXAFS analysis and do not intend to assume distributed binding.

Ligand types and numbers of the EXAFS model, together with metal-specific first-shell distances, match the experimental spectra (Figure 4 and Table 3). The first structural characterization of the plant GLX 2-2 active site therefore confirms its previous model, which has been solely based on sequence identities to the human enzyme with a known three-dimensional structure (*14*).

For all three metals, the first-shell oxygen and nitrogen distances were independently refined (Table 3). First-shell distances are 2.14 ± 0.01 Å for iron−histidine, 1.96 ± 0.01 Å for iron−oxygen, 2.26 ± 0.01 Å for manganese−histidine, 2.11 ± 0.01 Å for manganese−oxygen, 2.00 ± 0.02 Å for zinc−imidazole, and 1.98 ± 0.03 Å for zinc−oxygen. The metal−ligand distances match reference values found by a comprehensive analysis of high-resolution structures in the Cambridge Structural Database (*27*) and the Protein Data Bank (*29*) (Table 4). The iron−oxygen and manganese−oxygen distances are slightly shorter than reference distances for water molecules; however, they match reference distances for ligating carboxylate groups. This fits to the ligand stoichiometry of the structural model where most ligating oxygen ions are part of aspartate residues.

Reference coordination bond lengths are dependent on the coordination number but overlap within the error range for 5- and 6-fold coordination (*27*). In the case of iron, additional information on the coordination number and local symmetry can be deduced from the intensity of the iron preedge peak. The area was determined to be 6.2 units, which is typical for 6-fold iron coordination in ferric and diferric sites (*30*) (see below for determination of the iron oxidation state). EXAFS fits with 6-fold coordination have slightly elevated *R*-factors[3] (data not shown); however, 6-fold coordination is within the error range of the final EXAFS model. While the EXAFS model theoretically includes 4-, 5-, and 6-fold coordination, both the iron preedge size and comparison with the crystal structure of human glyoxalase II exclude 4-fold coordination and result in a final model of 5−6-fold coordination, eventually including a water ligand in addition to the coordination presented in Figure 1. The EXAFS analysis was at no point biased toward any of the typical coordination bond lengths. Hence, iron, manganese, and zinc are coordinated with their characteristic first-shell distances in the range of 2.0−2.3 $Å^{-1}$, indicative of structural flexibility in the GLX 2-2 active site.

The Debye−Waller factors (σ^2) for the first-shell ligands are elevated but still within the range observed for other proteins, such as the iron/zinc center of kidney bean purple acid phosphatase (*31*). The first-shell Debye−Waller factors reflect the disorder of the metal ligands for both binding sites. The present data analysis applies averaged distances to prevent overinterpretation of the data and is due to the fact that the major aim of this EXAFS study is to prove the metal binding to the active site.

The Fourier-transformed EXAFS spectra show a peak at about 3.2 Å distance which can be attributed to an adjacent

[3] The *R*-factor is used as a measure for the goodness of the fit and is defined by ref *1*. Smaller values indicate better fits.

Table 3: Coordination Spheres for Iron, Manganese, and Zinc as Derived by EXAFS Analysis[a]

			iron EXAFS		manganese EXAFS		zinc EXAFS	
Fermi energy offset (eV)			−1.7 (5)		−6.7 (6)		−2.5 (9)	
R-factor[3] (%)			27.8		23.7		36.5	
			∠M−N−C3: 115 (7)°		∠M−N−C3: 130 (9)°		∠M−N−C3: 125 (15)°	
ligand	atom	*N*	*r* (Å)	σ^2 (Å)	*r* (Å)	σ^2 (Å^2)	*r* (Å)	σ^2 (Å^2)
imidazole group,[b]	N		2.14 (1)	0.008 (1)	2.26 (1)	0.002 (1)	2.00 (2)	0.010 (3)
representing	C		*3.21*		*3.18*		*2.96*	
		2.5 (5)		0.006 (2)		0.004 (4)		0.009 (6)
His residue	C		*2.98*		*3.27*		*3.00*	
	C		*4.25*		*4.33*		*4.08*	
				0.008 (3)		0.002 (2)		0.009 (4)
	N		*4.18*		*4.40*		*4.13*	
	O	2.5 (5)	1.96 (1)	0.008 (1)	2.11 (1)	0.004 (2)	1.98 (4)	0.010 (3)
second metal[c] in dinuclear site		1.0 (2)	3.15 (5)	0.007 (2)	3.20 (4)	0.006 (3)	3.19 (6)	0.009 (3)
					average metal−metal distance: 3.18 (6)			

[a] *N* is the coordination number, *r* is the mean interatomic distance, and σ^2 is the Debye−Waller factor. ∠M−N−C3 describes the planar angle between the metal, the coordinating nitrogen, and the C3 atom of the imidazole group. Numbers in parentheses indicate the uncertainty of the last digit. The error range of the coordination number is based on a reference study (*28*). [b] Histidine residues are represented by an imidazole group as provided by EXCURV98 and used as a rigid body for constrained refinement. Only the distance to the ligating nitrogen atom is refined; the uncertainty of the distance is not calculated for outer shell imidazole atoms as indicated by italic letters. The coordination number of outer shell imidazole atoms is the same as for the coordinating first-shell nitrogen atom. Debye−Waller factors of outer shell imidazole atoms with similar distances to the metal center are refined collectively. The M−N−C3 angles are refined to partially compensate for inaccuracies of the rigid imidazole body. [c] The type of the neighboring metal is set to be one-third Fe, one-third Mn, and one-third Zn as this EXAFS analysis cannot distinguish between a neighboring iron, manganese, or zinc atom. The refined metal−metal distance only marginally depends on the type of the neighboring metal (0.01−0.03 Å); this is included in the respective error margin. As a consequence of the correlation between the Debye−Waller parameter and the coordination number, the metal−metal coordination number is 1.0 (2) despite substoichiometric metal occupancy (Table 2).

Table 4: Compliance of Characteristic First-Shell Distances with Experimental Values for Glyoxalase II[a]

		first-shell distance (Å)	
metal	ligand	characteristic	GLX 2 model
Fe(III)	oxygen (carboxylate)	2.01 (5)	1.96 (1)
	oxygen (water)	2.06 (6)	
	nitrogen (imidazole)	2.08−2.22[b]	2.14 (1)
Mn(II)	oxygen (carboxylate)	2.15 (7)	2.11 (1)
	oxygen (water)	2.19 (4)	
	nitrogen (imidazole)	2.19 (8)	2.26 (1)
Zn(II)	oxygen (carboxylate)	2.00 (7)	1.98 (3)
	oxygen (water)	2.06 (9)	
	nitrogen (imidazole)	2.00 (2)	2.00 (2)

[a] Typical metal−ligand distances are taken from an abundant analysis of small molecule crystallography (*27*) and further established by high-resolution protein structures (*29*); glyoxalase II metal ligation is as described in Table 3. Reference data for ligands that are relevant to this study have been listed for 6-fold coordination of iron and manganese and 5-fold coordination of zinc. Whenever available, the expected values for 5- and 6-fold coordination overlap within their error range. Numbers in parentheses indicate the uncertainty of the last digit. The EXAFS analysis was not biased toward any of the characteristic values. [b] Bimodal distribution: one group in the range of 1.95−1.99 Å and a second group in the range of 2.08−2.22 Å.

metal (Figure 4). EPR spectroscopy (see below) gives proof for dimetal centers such as Fe(III)Fe(II) and Mn(II)Mn(II). EXAFS fits including a neighboring metal yield lower *R*-factors; however, the decrease of about 4% cannot be considered to be significant. Thus, EXAFS analysis alone does not unambiguously prove an adjacent metal (Figure 4, thick black line for model with second metal and gray line for model without). Concerning zinc, which is EPR silent, EXAFS is still indicative for a metal−metal contribution; this is concluded from an EXAFS study on the mono- and dizinc forms of wild-type *Bacillus cereus* metallo-β-lactamase: the corresponding peak in the Fourier transform is only present in the dizinc form but missing in the monozinc case (*32*).

The element-specific metal−metal distances were refined independently and overlap within their error margins (Table 3), yielding an average distance of 3.18 ± 0.06 Å. This is well within the range of dinuclear metal sites with bridging carboxylate residues (*33*). EXAFS analysis, in contrast to EPR spectroscopy, could not distinguish between iron, manganese, or zinc for the neighboring metal. The correlation between the Debye−Waller parameter and the coordination number prevents the refinement of metal occupancies.

Iron and Manganese Oxidation State. The absorption edge shape and position can help to deduce the oxidation state of the absorbing metal. The typical Mn(II) feature is a narrow but intense absorption maximum (white line) directly at the rising edge (*34*). For higher oxidation states, this peak broadens and is shifted to higher energies. The absorption edge shape identifies Mn(II) for all glyoxalase II samples (Figure 2); this is also supported by EPR spectroscopy (see below). The shape of the iron absorption edges supports the predominant presence of ferric iron, as is deduced by comparison to the ferrous and ferric states of proteins such as soybean lipoxygenase-1 (*35*). The presence of iron in its ferric state complies well with the oxidative experimental conditions. Most likely, it does not reflect the *in vivo* iron oxidation state. Fractions of Fe(II) cannot be excluded since the shape of the iron absorption edge is a less distinctive marker of the oxidation state than in the case of manganese. For example, the absorption edge of ferrous catechol 2,3-dioxygenase lacks the typical sharp feature at the rising edge maximum (*36*). In fact, EPR spectroscopy gives evidence for iron being present as mostly Fe(III) and only to a lesser extent Fe(II) (see below).

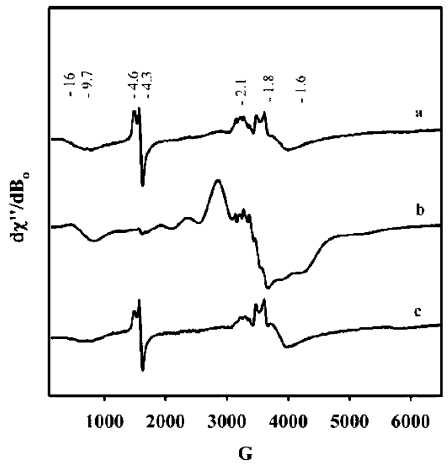

FIGURE 5: EPR spectra from GLX 2-2 preparations with different ratios of iron, manganese, and zinc: a, GLX 2-2 produced in standard medium; b, GLX 2-2 produced in manganese-enriched medium; c, GLX 2-2 produced in iron-enriched medium.

Summary of XAS Results. EXAFS analysis reveals the coordination of iron, manganese, and zinc to the glyoxalase II dinuclear active site with their element-specific, characteristic distances, indicating a structurally flexible binding site. The coordination number is 5−6. A conserved metal−metal distance of 3.18 ± 0.06 Å is determined for all three absorption edges. Manganese is present as Mn(II) and iron predominantly as Fe(III).

EPR Spectroscopy Identifies Several Different Types of Dinuclear Metal Sites

EPR spectroscopy yields information about the type and oxidation state of paramagnetic metal ions as well as the presence of spin-coupled dinuclear centers. Especially the capacity to directly identify spin-coupled dimetal centers is of great use for the present study. Since GLX 2-2 contains significant amounts of iron, manganese, and zinc, several types and combinations of mono- and dinuclear sites may exist, including mixed and EPR-silent sites.

The EPR spectrum of std-med GLX 2-2 at 4.7 K shows three distinct sets of signals: (I) two rhombic signals with g values of 4.6 and 4.3, (II) a broad signal centered at $g = 2.1$, which exhibits hyperfine splitting, and (III) a broad, rhombic signal at $g < 2$, with apparent g values of 1.9, 1.8, and 1.6 (Figure 5). The EPR spectrum of Fe-med GLX 2-2 is almost identical to that of std-med GLX 2-2. This result agrees nicely with the metal contents of Fe-med and std-med GLX 2-2. Manganese-enriched GLX 2-2 has a significantly different EPR spectrum.

Iron-Containing Centers. The position and shape of the $g = 4.6$ signals are typical for isolated, high-spin Fe(III) (*37*). This signal arises from the ground states $m_s = \pm^3/_2$; the very small feature at $g = 9.7$ corresponds to $m_s = \pm^1/_2$ states, which are only populated at very low temperatures (*38*, *39*). The $g = 9.7$ feature is missing at 20 and 30 K (data not shown). These properties are characteristic of uncoupled, high-spin Fe(III) centers in rhombically distorted environments and for Fe(III) in dinuclear Fe(III)Zn(II) centers (*38*, *39*). Std-med and Fe-med GLX 2-2 bind about 0.8 iron per protein. Spin quantitation on the $g = 4.6$ and 9.7 signals under nonsaturating conditions identified 0.1 iron per protein, suggesting that ∼10% of the std-med GLX 2-2 sample contains a dinuclear Fe(III)Zn(II) center. The minor signal at $g = 4.3$ is assigned as adventitous Fe(III) with greater rhombic distortion (*37*); this iron accounts for less than 10% of the total iron present. The EPR signals at $g < 2$ are consistent with the presence of a mixed-valence, antiferromagnetically coupled Fe(III)Fe(II) center ($S = {}^1/_2$) with rhombic distortion, reminiscent of the centers observed in the mammalian purple acid phosphatases (*39*−*41*), methane monooxygenase (*42*), and ribonucleotide reductase (*43*). This signal exhibits very strong temperature dependence and disappears at temperatures greater than 25 K (data not shown). Spin quantitation against a Cu(II) standard yields 0.15 spin/mol of protein, which is consistent with 0.3 mol of iron/mol of protein. This suggests that ∼40% of std-med and Fe-med GLX 2-2 contain an antiferromagnetically coupled Fe(III)Fe(II) center. The weak but broad signal at $g = 16$ is similar to a signal present in the mixed-valence dinuclear iron center in ribonucleotide reductase (*44*, perpendicular mode EPR at 4 K). It has been attributed to weak ferromagnetic coupling between high-spin ferrous iron ions or to mononuclear, high-spin ferrous sites (*44* and references cited therein). However, our experimental setup does not allow the detection of mononuclear ferrous iron, and the origin of the $g = 16$ signal remains ambiguous. Combining the amounts of iron calculated in the Fe(III)Zn(II) and Fe(III)Fe(II) centers, ∼50% of the iron in std-med GLX 2-2 is EPR active. The remaining iron may persist as part of $S = 0$, spin-coupled centers, such as Fe(III)Mn(II) or as mononuclear ferrous iron. Noteworthy, the *in vivo* iron oxidation state is likely to be altered due to the oxidative experimental conditions; the persistence of mononuclear ferrous iron is therefore considered to be unlikely.

Manganese-Containing Centers. The EPR spectra of std-med and Fe-med GLX 2-2 show a broad signal centered at $g = 2.1$, which is split into at least six lines with a hyperfine constant $A = 38$ G. This is indicative of ^{55}Mn(II) ($I = {}^5/_2$). The $g = 2.1$ signal rules out mixed-valence dinuclear manganese centers, which are expected to yield overlapping, multiline signals. The hyperfine constant is similar to that of Mn(II)Fe(II) or Mn(II)Mn(II) centers, such as the spin-coupled iron−manganese center in $[Fe^{II}Mn^{II}BPMP(O_2CCH_2CH_3)_2](BPh_3)$ (*45*) or the ferromagnetically coupled dimanganese center in Mn(II)Mn(II) catalase ($S = 5$) (*46*, *47*).

The presence of mononuclear Mn(II) or Mn(II)Zn(II) centers can neither be confirmed nor be ruled out: while the hyperfine constant $A = 38$ G is not indicative of mononuclear Mn(II) or Mn(II)Zn(II) centers, a much smaller six-line pattern with larger hyperfine splitting ($A \sim 90$ G) is possibly present with low intensity and unresolved from the major features at $g = 2.1$ and $g < 2$. To determine whether the Mn(II) signal of std-med/Fe-med GLX 2-2 is due to Fe(II)Mn(II) or Mn(II)Mn(II) centers, the temperature dependence properties of the $g = 2.1$ signal were explored. The EPR signal of $[Fe^{II}Mn^{II}BPMP(O_2CCH_2CH_3)_2](BPh_3)$ is attributed to transitions in the ground state $M_s = \pm^1/_2$ spin levels (*45*), and at 20 K, there is a new resonance at $g = 5.5$, corresponding to transitions in the excited $M_s = +^3/_2$ spin level. The GLX 2-2 Mn(II) signal shows no new features at 30 K (data not shown), which suggests vastly differing zero-field splittings between the model complex and the Mn(II) in GLX 2-2 (*48*). The GLX 2-2 samples therefore do not contain Fe(II)Mn(II) centers, and the $g = 2.1$ signal is

attributed to Mn(II)Mn(II) centers. This is supported by comparing the std-med/Fe-med GLX 2-2 EPR spectra with the Mn(II)Mn(II) catalase spectrum (*46*, *47*). The catalase spectrum shows a broad, multiline signal extending over 4000 G with peak separations of 430 and 730 G; one or more of the lines is split into 6−11 lines due to hyperfine interactions (*46*, *47*). The std-med/Fe-med EPR spectra also show a broad, low-intensity signal extending over 4000 G. At 30 K, the hyperfine splitting signal at $g = 2.1$ remains present (data not shown). Manganese-enriched GLX 2-2 has an EPR spectrum closely similar to that of Mn(II)Mn(II) catalase with peak separations of 440 and 750 G. Taken together, the GLX 2-2 EPR spectra reveal the presence of ferromagnetically coupled Mn(II)Mn(II) centers. Spin quantitation of the entire Mn(II) signal in the std-med/Fe-med spectra is not possible, since it is overlapped by the Fe(III) and Fe(III)Fe(II) signals, but a lower limit can be determined by quantitating the $g = 2.1$ feature and comparison with the manganese-enriched sample. With Mn(II) and Cu(II) as spin standards, the $g = 2.1$ signal integrates to 0.08 Mn(II) per protein. Thus ∼30% of the total manganese in std-med/Fe-med GLX 2-2 is present as ferromagnetically coupled Mn(II)Mn(II) centers.

Summary of EPR Results. The EPR studies indicate that std-med and Fe-med GLX 2-2 have a variety of metal centers, and about 50% of these centers are EPR active; these include Fe(III)Fe(II), Fe(III)Zn(II), and Mn(II)Mn(II) centers. The presence of Mn(II)Zn(II) centers remains ambiguous. Spin quantitation shows that ∼40% of the total iron in std-med/Fe-med GLX 2-2 is part of mixed-valence, antiferromagnetically coupled Fe(III)Fe(II) centers; ∼10% belongs to Fe(III)Zn(II) centers, and ∼30% of the total manganese in std-med/Fe-med GLX 2-2 is part of ferromagnetically coupled Mn(II)Mn(II) centers. Manganese-enriched GLX 2-2 has an EPR spectrum closely reminiscent of Mn(II)Mn(II) catalase. The *in vivo* iron oxidation state is likely to be altered by the oxidative experimental conditions; this could explain the absence of EPR-active Fe(II)Mn(II) centers. Since EPR spectroscopy reveals most of the possible EPR-active dimetal centers, we predict that analogously most of the EPR-silent dimetal centers also occur.

DISCUSSION

This work characterizes heterogeneous samples of glyoxalase II to better understand the *in vivo* metal utilization in the enzyme. Iron, manganese, and zinc are bound to the dinuclear active site of GLX2-2, with different ratios yielding similar catalytic efficiencies. Various types of metal−metal combinations are incorporated *in vivo*. Therefore, recombinant GLX 2-2 is the only member of the metallo-β-lactamase superfamily to be isolated with significant amounts of iron, manganese, and zinc. EXAFS spectroscopy suggests a structural basis for the broad metal selectivity: iron, manganese, and zinc are coordinated with their optimal bond lengths, hence proving a high degree of structural flexibility within the GLX 2-2 dinuclear active site (Table 4). Site-specific binding of individual metals is not detected with our experimental methods. EPR spectroscopy reveals the presence of Mn(II)Mn(II) centers, thus indicating that manganese is distributed between the two binding sites. These findings are consistent with recent reports on other members of the metallo-β-lactamase superfamily (*32*): in the monozinc form of the *B. cereus* II metallo-β-lactamase it has been shown that the sole metal ion is distributed between the two binding sites. The presence of Fe(III)-Fe(II) centers may be indicative of a tri- and a bivalent iron binding site. The experimental conditions are, however, likely to have altered the *in vivo* iron oxidation state, and the presence of Fe(II)Fe(II) centers can be assumed for the physiological conditions. Glyoxalase II yields similar catalytic efficiencies (k_{cat}/K_M) with different ratios of active site bound iron, manganese, and zinc. In the case of Mn-med GXL 2-2, there is an apparent correlation between the decrease of both k_{cat} and K_M by approximately one-half and the respective decrease of the iron content. However, the present metal composition does not allow us to firmly establish the catalytic efficiency of individual metal types and different metal−metal combinations. The similar catalytic efficiencies (k_{cat}/K_M) of Mn-med GLX 2-2 with less than 0.1 zinc and std-med GLX 2-2 with 0.4 zinc per protein demonstrate that glyoxalase II does not rely on zinc for its catalytic activity. There are numerous examples of zinc-dependent hydrolytic enzymes where zinc can be replaced in vitro by other transition metals with maintained enzymatic activity (*49*).

The combination of 5−6-fold coordination with 2−3 ligating histidine residues structurally classifies *A. thaliana* GLX 2-2 as a typical zinc binding protein and not one that binds predominantly iron and manganese. Most other members of the metallo-β-lactamase superfamily are purified with approximately two zinc ions per protein when produced as soluble recombinant protein in *E. coli*. This is the case for the L1 metallo-β-lactamase from *Stenotrophomonas maltophila* (*50*), CcrA metallo-β-lactamase from *Bacteroides fragilis* (*51*), and FEZ-1 metallo-β-lactamase from *Legionella gormanii* (*52*). In contrast, zinc phosphodiesterase, a new *E. coli* member of the metallo-β-lactamase superfamily, contains very little metal in the as isolated form when overexpressed in *E. coli* but requires two zinc ions for full phosphodiesterase activity (*20*). GLX 2-2 with its significant amounts of iron, manganese, and zinc is unique within the metallo-β-lactamase superfamily. It appears that the catalytic and metal binding properties of GLX 2-2 allow full functionality with various types and ratios of bound metal ions. For a number of protein phosphatases the nature of the metal ions forming the dinuclear site (iron, manganese, or zinc) has also not been firmly established (*53*). Clearly, many details remain to be elucidated about metal selectivity *in vivo* and metal incorporation into protein binding sites. Factors in addition to structural properties of the metal binding site are involved in protein metal binding, including specific metallochaperones (*54*, *55*), and protein properties outside the metal binding site. The GLX 2-2 R248W mutant is isolated as a dizinc protein with significantly altered metal content in comparison to wild-type GLX 2-2 (*11*). In the crystal structure of human glyoxalase II (*14*), the corresponding residue is located at a distance of >17 Å from the metal binding site. Taken together, comparison of our results with those from homologously produced *E. coli* zinc phosphodiesterase (*20*) and heterologously produced L1 and FEZ-1 (*50*, *52*), as well as the GLX 2-2 R248W mutant (*11*), demonstrates that the *in vivo* metal selectivity of the metallo-β-lactamase domain does not exclusively depend on the local metal binding site.

Our results on recombinant GLX 2-2 may only partially reflect the situation of the native enzyme. No information is available on the metal content of a GLX 2 enzyme purified from a native source. The absence of further 3d transition metals, copper, nickel, and cobalt, is consistent with the observation that copper proteins are almost exclusively located outside the cytoplasm [*56* (page 419)] and that specific metallochaperones guide copper and nickel incorporation into proteins (*54*, *55*). Generally, both nickel and cobalt are present far less in metalloproteins than iron, manganese, zinc, or copper [*56* (page 437), *57*].

GLX 2-2 represents a case where *in vivo* a metalloenzyme is produced with a variety of dimetal centers yielding similar enzymatic activities. Possibly, some flexibility regarding the metal requirement for a biochemical process makes a biological system less vulnerable to fluctuations in the environmental metal supply. This complements the undoubtedly enormous capability of biological systems to distinguish between different types of metal ions and to achieve their selective incorporation and usage (*58*). The diverse properties of different metal types, e.g., in redox processes or their ionic radii, evidently impose a strict limit on their flexible usage. Yet, there may be significant practical consequences, e.g., in the area of structure-based drug design for metalloproteins.

ACKNOWLEDGMENT

We thank Professor Russ Hille and Craig Hemann at The Ohio State University for their assistance in collecting the EPR spectra.

SUPPORTING INFORMATION AVAILABLE

One table giving EXAFS model fits without an adjacent metal ion for iron, manganese, and zinc. This material is available free of charge via the Internet at http://pubs.acs.org.

REFERENCES

1. Binsted, N., Strange, R. W., and Hasnain, S. S. (1992) *Biochemistry 31*, 12117−12125.
2. Thornalley, P. J. (1995) *Crit. Rev. Oncol. Hematol. 20*, 99−128.
3. Thornalley, P. J. (1998) *Chem-Biol. Interact. 112*, 137−151.
4. Papoulis, A., Al-Abed, Y., and Bucala, R. (1995) *Biochemistry 34*, 648−655.
5. Rahman, A., Shahabuddin, A., and Hadi, S. M. (1990) *J. Biochem. Toxicol. 5*, 161−166.
6. Lo, T. W. C., Westwood, M. E., McLellan, A. C., Selwood, T., and Thornalley, P. J. (1994) *J. Biol. Chem. 269*, 32299−32305.
7. Thornalley, P. J. (1993) *Mol. Aspects Med. 14*, 287−371.
8. Rulli, A., Carli, L., Romani, R., Baroni, T., Giovannini, E., Rosi, G., and Talesa, V. (2001) *Breast Cancer Res. Treat. 66*, 67−72.
9. Allen, R. E., Lo, T. W. C., and Thornalley, P. J. (1993) *Biochem. Soc. Trans. 21*, 535−540.
10. Norton, S. J., Elia, A. C., Chyan, M. K., Gillis, G., Frenzel, C., and Principato, G. B. (1993) *Biochem. Soc. Trans. 21*, 545−549.
11. Crowder, M. W., Maiti, M. K., Banovic, L., and Makaroff, C. A. (1997) *FEBS Lett. 418*, 351−354.
12. Ullah, J. H., Walsh, T. R., Taylor, I. A., Emery, D. C., Verma, C. S., Gamblin, S. J., and Spencer, J. (1998) *J. Mol. Biol. 284*, 125−136.
13. Concha, N. O., Rasmussen, B. A., Bush, K., and Herzberg, O. (1996) *Structure 4*, 823−836.
14. Cameron, A. D., Ridderstrom, M., Olin, B., and Mannervik, B. (1999) *Struct. Folding Des. 7*, 1067−1078.
15. Ridderstrom, M., Cameron, A. D., Jones, T. A., and Mannervik, B. (1997) *Biochem. J. 328*, 231−235.
16. Ridderstrom, M., Cameron, A. D., Jones, T. A., and Mannervik, B. (1998) *J. Biol. Chem. 273*, 21623-21628.
17. Ridderstrom, M., Jemth, P., Cameron, A. D., and Mannervik, B. (2000) *Biochim. Biophys. Acta 1481*, 344−348.
18. Zang, T. M., Hollman, D. A., Crawford, P. A., Crowder, M. W., and Makaroff, C. A. (2001) *J. Biol. Chem. 276*, 4788−4795.
19. Wang, Z., Fast, W., Valentine, A. M., and Benkovic, S. J. (1999) *Curr. Opin. Chem. Biol. 3*, 614−622.
20. Vogel, A., Schilling, O., Niecke, M., Bettmer, J., and Meyer-Klaucke, W. (2002) *J. Biol. Chem. 277*, 29078−29085.
21. Frazao, C., Silva, G., Gomes, C. M., Matias, P., Coelho, R., Sieker, L., Macedo, S., Liu, M. Y., Oliveira, S., Teixeira, M., Xavier, A. V., Rodrigues-Pousada, C., Carrondo, M. A., and Le Gall, J. (2000) *Nat. Struct. Biol. 7*, 1041−1045.
22. Edelhoch, H. (1967) *Biochemistry 6*, 1948−1954.
23. Pettifer, R. F., and Hermes, C. (1985) *J. Appl. Crystallogr. 18*, 404−412.
24. Roe, A. L., Schneider, D. J., Mayer, R. J., Pyrz, J. W., Widom, J., and Que, L. (1984) *J. Am. Chem. Soc. 106*, 1676−1681.
25. Ridderstrom, M., and Mannervik, B. (1997) *Biochem. J. 322*, 449−454.
26. Ridderstrom, M., Saccucci, F., Hellman, U., Bergman, T., Principato, G., and Mannervik, B. (1996) *J. Biol. Chem. 271*, 319−323.
27. Harding, M. M. (1999) *Acta Crystallogr. D 55*, 1432−1443.
28. Eggers-Borkenstein, P., Priggemeyer, S., Krebs, B., Henkel, G., Simonis, U., Pettifer, R. F., Nolting, H. F., and Hermes, C. (1989) *Eur. J. Biochem. 186*, 667−675.
29. Harding, M. M. (2001) *Acta Crystallogr. D 57*, 401−411.
30. Westre, T. E., Kennepohl, P., DeWitt, J. G., Hedman, B., Hodgson, K. O., and Solomon, E. I. (1997) *J. Am. Chem. Soc. 119*, 6297−6314.
31. Priggemeyer, P., Eggers-Borkenstein, F., Ahlers, B. Krebs, G. Henkel, M. Körner, H. Witzel, Nolting, H.-F., and Hermes, C. (1995) *Inorg. Chem. 34*, 1445−1454.
32. de Seny, D., Heinz, U., Wommer, S., Kiefer, M., Meyer-Klaucke, W., Galleni, M., Frere, J. M., Bauer, R., and Adolph, H. W. (2001) *J. Biol. Chem. 276*, 45065−45078.
33. Wilcox, D. E. (1996) *Chem. Rev. 96*, 2435−2458.
34. Stemmler, T. L., Sossong, T. M., Jr., Goldstein, J. I., Ash, D. E., Elgren, T. E., Kurtz, D. M., Jr., and Penner-Hahn, J. E. (1997) *Biochemistry 36*, 9847−9858.
35. Van der Heijdt, L. M., Feiters, M. C., Navaratnam, S., Nolting, H. F., Hermes, C., Veldink, G. A., and Vliegenthart, J. F. (1992) *Eur. J. Biochem. 207*, 793−802.
36. Bertini, I., Briganti, F., Mangani, S., Nolting, H. F., and Scozzafava, A. (1994) *Biochemistry 33*, 10777−10784.
37. Palmer, G. (1985) *Biochem. Soc. Trans. 13*, 548−560.
38. Yu, L., Haddy, A., and Rusnak, F. (1995) *J. Am. Chem. Soc. 117*, 10147−10148.
39. David, S. S., and Que, L. (1990) *J. Am. Chem. Soc. 112*, 6455−6463.
40. Crowder, M. W., Vincent, J. B., and Averill, B. A. (1992) *Biochemistry 31*, 9603−9608.
41. Vogel, A., Spener, F., and Krebs, B. (2001) in *Handbook of Metalloproteins* (Messerschmidt, A., Huber, R., Poulos, T., and Wieghardt, K., Eds.) pp 752−767, John Wiley & Sons, Chichester.
42. Davydov, R., Valentine, A. M., Komar-Panicucci, S., Hoffman, B. M., and Lippard, S. J. (1999) *Biochemistry 38*, 4188−4197.
43. Davydov, R., Kuprin, S., Graslund, A., and Ehrenberg, A. (1994) *J. Am. Chem. Soc. 116*, 11120−11128.
44. Atta, M., Debaecker, N., Andersson, K. K., Latour, J.-M., Thelander, L., and Graeslund, A. (1996) *J. Biol. Inorg. Chem. 1*, 210−220.
45. Holman, T. R., Wang, Z., Hendrich, M. P., and Que, L. (1995) *Inorg. Chem. 34*, 134−139.
46. Mathur, P., Crowder, M., and Dismukes, G. C. (1987) *J. Am. Chem. Soc. 109*, 5227−5233.
47. Pessiki, P. J., Khangulov, S. V., Ho, D. M., and Dismukes, G. C. (1994) *J. Am. Chem. Soc. 116*, 891−897.
48. Brudvig, G. W. (1995) in *Methods in Enzymology*, p 536, Academic Press, New York.
49. Lipscomb, W. N., and Sträter, N. (1996) *Chem. Rev. 96*, 2375−2433.
50. Crowder, M. W., Walsh, T. R., Banovic, L., Pettit, M., and Spencer, J. (1998) *Antimicrob. Agents Chemother. 42*, 921−926.

51. Wang, Z., and Benkovic, S. J. (1998) *J. Biol. Chem. 273*, 22402−22408.
52. Mercuri, P. S., Bouillenne, F., Boschi, L., Lamotte-Brasseur, J., Amicosante, G., Devreese, B., van Beeumen, J., Frere, J. M., Rossolini, G. M., and Galleni, M. (2001) *Antimicrob. Agents Chemother. 45*, 1254−1262.
53. Voegtli, W. C., White, D. J., Reiter, N. J., Rusnak, F., and Rosenzweig, A. C. (2000) *Biochemistry 39*, 15365−15374.
54. Rosenzweig, A. C. (2002) *Chem. Biol. 9*, 673−677.
55. O'Halloran, T. V., and Culotta, V. C. (2000) *J. Biol. Chem. 275*, 25057−25060.
56. Williams, R. J. P., and Fraústo da Silva, J. J. R. (2001) *The biological chemistry of the elements: the inorganic chemistry of life*, 2nd ed., Oxford University Press, Oxford and New York.
57. Kobayashi, M., and Shimizu, S. (1999) *Eur. J. Biochem. 261*, 1−9.
58. Williams, R. J. P., and Fraústo da Silva, J. J. R. (2000) *Coord. Chem. Rev. 200−202*, 247−348.

BI034672O